

Gaugino Anomaly Mediated SUSY Breaking: phenomenology and prospects for the LHC

Howard Baer^{1*}, Senarath de Alwis^{2†}, Kevin Givens^{2‡},
Shibi Rajagopalan^{1‡}, Heaya Summy^{1§}

1. *Dept. of Physics and Astronomy, University of Oklahoma, Norman, OK 73019, USA*
2. *Dept. of Physics, University of Colorado, Boulder CO 80309, USA*

Abstract

We examine the supersymmetry phenomenology of a novel scenario of supersymmetry (SUSY) breaking which we call Gaugino Anomaly Mediation, or inoAMSB. This is suggested by recent work on the phenomenology of flux compactified type IIB string theory. The essential features of this scenario are that the gaugino masses are of the anomaly-mediated SUSY breaking (AMSB) form, while scalar and trilinear soft SUSY breaking terms are highly suppressed. Renormalization group effects yield an allowable sparticle mass spectrum, while at the same time avoiding charged LSPs; the latter are common in models with negligible soft scalar masses, such as no-scale or gaugino mediation models. Since scalar and trilinear soft terms are highly suppressed, the SUSY induced flavor and CP -violating processes are also suppressed. The lightest SUSY particle is the neutral wino, while the heaviest is the gluino. In this model, there should be a strong multi-jet $+E_T^{\text{miss}}$ signal from squark pair production at the LHC. We find a 100 fb^{-1} reach of LHC out to $m_{3/2} \sim 118 \text{ TeV}$, corresponding to a gluino mass of $\sim 2.6 \text{ TeV}$. A double mass edge from the opposite-sign/same flavor dilepton invariant mass distribution should be visible at LHC; this, along with the presence of short- but visible- highly ionizing tracks from quasi-stable charginos, should provide a smoking gun signature for inoAMSB.

*Email: baer@nhn.ou.edu

†Email: dealwiss@colorado.edu

‡Email: kevin.givens@colorado.edu

‡Email: shibi@nhn.ou.edu

§Email: heaya@nhn.ou.edu

1 Introduction

String theory is very attractive in that it allows for a consistent quantum mechanical treatment of gravitation, while at the same time including all the necessary ingredients for containing the well-known gauge theories which comprise the Standard Model of particle physics. Phenomenologically viable versions of string theory require the stabilization of all moduli fields as well as weak to intermediate scale supersymmetry breaking. Models satisfying these criteria were first developed in the context of type IIB string theory using flux compactifications and non-perturbative effects on Calabi Yau orientifolds (CYO's) (for reviews see [1] [2]). The low energy limit of type-IIB string theory after compactification on a CYO is expected to be $N = 1$ supergravity (SUGRA).

Two classes of the above models which yield an interesting supersymmetry breaking scenario have been studied:

- a) Those with only a single Kähler modulus (SKM models). These are essentially of the KKLT type [3] but with uplift coming from one-loop quantum effects.
- b) Large Volume Scenario (LVS)[4] models which require at least two moduli.

In both of these types of models, the moduli fields are stabilized using a combination of fluxes and non-perturbative effects. Additionally, supersymmetry is broken by the moduli fields acquiring non-zero F-terms and interacting gravitationally with the MSSM. For both models, the gauginos acquire mass predominately through a Weyl anomaly effect while the classical contribution to the scalar masses and trilinear coupling constants are naturally suppressed.

Generically in a string model there are three types of contributions to the soft SUSY breaking terms:

1. Terms generated by classical string theory effects.
2. Terms generated by quantum effects (effectively string loop corrections).
3. Weyl anomaly (AMSB) contributions[5] to the gaugino masses.

In this class of models, the MSSM may be located on D3 branes at a singularity or on D7 branes wrapping a collapsing four cycle in the CYO. The string theory calculations are expected to give boundary conditions at (or near) the string scale M_{string} , which may range (almost) up to the GUT scale or as low as some intermediate scale $\ll M_{GUT}$. In both cases, the classical string theory as well as 1-loop quantum contributions to the soft SUSY breaking terms are suppressed relative to the weak scale. For gaugino masses, it has been shown that these will gain contributions from the Weyl anomaly, and therefore assume the usual form as expected in models with anomaly-mediated SUSY breaking:

$$M_i = \frac{b_i g_i^2}{16\pi^2} m_{3/2}. \quad (1)$$

Here i labels the gauge group, g_i is the associated gauge coupling, $m_{3/2}$ is the gravitino mass, and b_i is the co-efficient of the gauge group beta function: $b_i = (33/5, 1, -3)$. Meanwhile, soft

SUSY breaking scalar masses will have generically suppressed classical string masses and 1-loop contributions, and receive *no contribution* from Weyl anomalies[6].

To good approximation, we can set in this class of models,

$$m_0 = A_0 = 0, \tag{2}$$

where m_0 is the common soft SUSY breaking scalar mass at M_{string} and A_0 is the trilinear soft SUSY breaking (SSB) term.

In addition, the bilinear SSB mass B and the superpotential μ term would be zero at the classical (AdS) minimum. However these can acquire non-zero values once uplift terms that correct the value of the cosmological constant are turned on. Here, we will feign ignorance as to the origin of these terms, and instead adopt a phenomenological approach which determines their values by finding an appropriate minimum of the electroweak scalar potential. The minimization procedure allows one to trade the B parameter for the ratio of Higgs field vevs $\tan \beta$, and to require the value of $|\mu|$ which is needed in order to specify the correct mass of the Z boson[7]. In this case, the SKM and LVS models would both be well-described by the following parameter space

$$m_{3/2}, \tan \beta, \text{sign}(\mu), \tag{3}$$

where in addition we take $m_0 = A_0 = 0$. While the SSB scalar and trilinear terms are small at M_{string} , they can become large at $Q = M_{weak}$ due to renormalization group (RG) running.

In fact, these sort of RG boundary conditions are similar to those of no-scale supergravity models (NS)[8], and also gaugino-mediated SUSY breaking (inoMSB) models[9]. However, in both NS and inoMSB models, it is expected that the gaugino masses unify to a common gaugino mass $m_{1/2}$ at the string scale. The fact that both scalar and trilinear soft SUSY breaking terms have only small contributions at the high scale (compactification scale M_c , M_P or M_{GUT}) is highly desirable for solving the SUSY flavor and CP problems. In the general MSSM, unconstrained off-diagonal terms in the scalar and trilinear sector lead to large contributions to flavor changing and CP violating processes, for which there are tight limits[10]. Under renormalization group evolution, the off-diagonal terms remain small, while diagonal terms receive significant contributions due to gauge interactions and the large gaugino masses.

Using the NS or inoMSB boundary conditions, it is well known that one gains a sparticle mass spectrum with τ sleptons as the lightest SUSY particle (LSP)¹. In models with R -parity conservation, the $\tilde{\tau}_1$ would be absolutely stable, thus violating constraints coming from search experiments for long lived, stable charged relics from the Big Bang. One way around this dilemma has been suggested by Schmaltz and Skiba[11]: adopting $M_{string} > M_{GUT}$, so that above-the-GUT-scale running lifts the value of m_0 above zero at the GUT scale. Another possibility is to allow for unconstrained, or a less-constrained, form of *non-universal* gaugino masses[12].

We find here that the $m_0 \sim A_0 \sim 0$ boundary conditions– along with the AMSB form for gaugino masses– in fact leads to viable sparticle mass spectra across most of parameter space, without the need for above-the-GUT-scale running, or a less-constrained form for gaugino masses, or an artificially light gravitino mass. While these boundary conditions seem to emerge

¹ One way out is to hypothesize the gravitino as LSP. In our case, we will find that the gravitino mass is always in the multi-TeV range.

naturally in type IIB string models with flux compactifications, we may also consider such boundary conditions by themselves as being perhaps more general, and well-motivated by their desirable low energy features. For this reason, we will hereafter refer to the class of models leading to the above boundary conditions as gaugino anomaly mediated SUSY breaking, or *inoAMSB* models, since only the gaugino masses receive contributions of the AMSB form, and the other soft parameters are similar to those as generated in gaugino mediation.

The remainder of this paper is organized as follows. In Sec. 2, we review some of the string theoretic supergravity model details that motivate us to consider the *inoAMSB* form of boundary conditions. In Sec. 3, we plot out the spectra of superpartners that is expected in the *inoAMSB* model. While some features are similar to what is known as “minimal” AMSB (mAMSB), some crucial differences exist that may allow one to distinguish *inoAMSB* from mAMSB and also “hypercharged” anomaly-mediation (HCAMSB)[13]. We also examine what happens if the string scale is taken to be some intermediate value, or if some small universal scalar mass is adopted. We also plot out low energy constraints from $BF(b \rightarrow s\gamma)$ and $(g-2)_\mu$. In Sec. 4, we examine the sort of signatures expected from the *inoAMSB* model at the CERN LHC. Since squark masses are always lighter than gluinos, we expect a large rate for $\tilde{q}\tilde{q}$ and $\tilde{q}\tilde{g}$ production, leading to a large rate for multi-jet+ E_T^{miss} events. Since the lightest SUSY particle is a neutral wino, as in most AMSB-type models, we expect a nearly mass degenerate, quasi-stable chargino, which can lead to short but observable highly ionizing tracks in a collider detector. In addition, squarks cascade decay to neutralinos, followed by neutralino decay to lepton plus either left- or right-slepton states. The unique cascade decay pattern leads to a distinct double mass edge in the same-flavor/opposite-sign dilepton invariant mass distribution, which distinguishes *inoAMSB* from mAMSB or HCAMSB. In Sec. 5, we present our conclusions.

2 Effective supergravity from IIB strings: Overview of Models

2.1 Effective Supergravity Theory

The low energy limit of IIB string theory, after compactification on a Calabi-Yao orientifold, yields $\mathcal{N} = 1$ supergravity. The (superspace) action then has the generic form (see for example [14, 15])

$$S = -3 \int d^8z \mathbf{E} \exp\left[-\frac{1}{3}K(\Phi, \bar{\Phi}; C, \bar{C}e^{2V})\right] + \left(\int d^6z 2\mathcal{E}[W(\Phi, C) + \frac{1}{4}f_a(\Phi)\mathcal{W}^a\mathcal{W}^a] + h.c.\right), \quad (4)$$

where we have set $M_P = (8\pi G_N)^{-1/2} = 2.4 \times 10^{18} GeV = 1$. Here K –the Kähler potential–is a real superfield as is the gauge pre-potential V . W –the superpotential–is a holomorphic field, as is the gauge coupling function f_a and the (fermionic) gauge (super) field strength $\mathcal{W}(V)$. $\mathbf{E}d^8z$ is the full superspace measure and $\mathcal{E}d^6z$ is the chiral superspace measure. Ignoring the D -terms, which are zero at the minimum of the potential in the class of models considered here,

the SUGRA potential takes the standard form (after going to the Einstein frame)

$$V(\Phi) = F^A F^{\bar{B}} K_{A\bar{B}} - 3|m_{3/2}(\Phi)|^2. \quad (5)$$

Here $F^A = e^{K/2} K^{A\bar{B}} D_{\bar{B}} W$, $D_A W \equiv \partial_A W + K_A W$ where $K_A = \partial_A K$, $K_{A\bar{B}} = \partial_A \partial_{\bar{B}} K$ and $|m_{3/2}|^2 \equiv e^K |W|^2$ becomes the squared gravitino mass when evaluated at the minimum of the potential.

We separate the chiral superfields of the theory into moduli fields (which come from string theory and describe the internal geometry of the CY manifold) and the dilaton (which are collectively called Φ) and the MSSM fields (which we have called C). Expanding K and W in powers of the MSSM fields we have:

$$W = \hat{W}(\Phi) + \mu(\Phi) H_d H_u + \frac{1}{6} Y_{\alpha\beta\gamma}(\Phi) C^\alpha C^\beta C^\gamma + \dots, \quad (6)$$

$$K = \hat{K}(\Phi, \bar{\Phi}) + \tilde{K}_{\alpha\bar{\beta}}(\Phi, \bar{\Phi}) C^\alpha C^{\bar{\beta}} + [Z(\Phi, \bar{\Phi}) H_d H_u + h.c.] + \dots \quad (7)$$

$$f_a = f_a(\Phi). \quad (8)$$

Here we have separated the two Higgs superfield multiplets ($H_{d,u}$). The moduli fields essentially play the role of spurion fields that break supersymmetry, once they are stabilized and acquire a definite vacuum expectation value such that one or more of them also has a non-zero F-term.

Also

$$\hat{K} = -2 \ln \left(\mathcal{V} + \frac{\hat{\xi}}{2} \right) - \ln \left(i \int \Omega \wedge \bar{\Omega}(U, \bar{U}) \right) - \ln(S + \bar{S}), \quad \text{and} \quad (9)$$

$$\hat{W} = \int G_3 \wedge \Omega + \sum_i A_i e^{-a_i T^i}. \quad (10)$$

Here \mathcal{V} is the volume of the CYO and is a function of the Kähler moduli superfields T^i (with $i = 1, \dots, h_{11}$), and $\hat{\xi}$ is a stringy (α') correction that is an $O(1)$ number depending on the Euler character of the CYO and the real part of the dilaton superfield S . Ω is the holomorphic three form on the CYO and is a function of the complex structure moduli superfields U_r (with $r = 1, \dots, h_{21}$).

2.2 Single Kähler modulus scenario

In this construction, type IIB string theory is compactified on a CYO and the MSSM lives on a stack of D3 branes. We take a CYO with just one Kähler modulus, T , (i.e. $h_{11} = 1$) but with a number $\sim 10^2$ of complex moduli, U_r . These moduli, along with the axio-dilaton, S , are then stabilized using internal fluxes and non-perturbative effects. Classically, we can find a minimum of this potential with the F -term of T being $\sim m_{3/2}$ with the other moduli F -terms being suppressed. The cosmological constant would be negative but suppressed. The soft terms are also highly suppressed. This solution of course receives quantum mechanical corrections starting at 1-loop. In terms of an effective field theory description, they would depend on a string scale cutoff Λ . These can serve to uplift the cosmological constant and to generate the soft SUSY breaking masses, proportional to $\frac{\Lambda}{4\pi} m_{3/2}$. The cutoff Λ is essentially the string scale and in this class of models may be taken as large as $10^{-2} M_P$ so that a GUT scenario could be accommodated. This class of models is discussed in [16].

2.3 Large Volume Scenario (LVS)

In this class of models[4], we again compactify IIB string theory on a CYO. However, we now consider more than one Kähler modulus, $T^i (i = 1, \dots, h_{11})$. In particular– in the simplest such situation– we have a large modulus, τ_b , and small moduli, (τ_s, τ_a) , controlling the overall size of the CYO and the volume of two small 4-cycles respectively. The total volume is then given by

$$\mathcal{V} = \tau_b^{3/2} - \tau_s^{3/2} - \tau_a^{3/2}. \quad (11)$$

This is referred to as a “Swiss Cheese” model. Again the MSSM may be located on D3 branes at a singularity. Alternatively, we could have it on a stack of D7 branes wrapping a four cycle (taken to be the one labelled by the index a). In this case, it has been argued [17, 18] that the necessity of having chiral fermions on this brane prevents this cycle from being stabilized by non-perturbative effects and it shrinks below the string scale. Effectively, this means that the physics is the same as in the D3 brane case.

Extremizing the potential leads to an exponentially large volume[4] $\mathcal{V} \sim e^{a\tau_s}$, $\tau_s \sim \hat{\xi}$. It turns out that the suppression of FCNC effects lead to $\mathcal{V} \gtrsim 10^5 l_P^6$ [19] (where l_P is the Planck length), so the string scale is $M_{string} \lesssim M_P/\sqrt{\mathcal{V}} \sim 10^{15.5} \text{GeV}$. The minimum of the potential (CC) is given by $V_0 \sim -\frac{m_{3/2}^2 M_P^2}{\ln m_{3/2} \mathcal{V}}$. This minimum can be uplifted to zero when S and U_r acquire (squared) F -terms of the order $\frac{m_{3/2}^2 M_P^2}{\ln m_{3/2} \mathcal{V}}$. Classical contributions to the scalar and slepton masses are also of this same order. With the above lower bound on the volume, this means that even for $m_{3/2} \sim 100 \text{ TeV}$, the classical soft terms are $\lesssim 100 \text{ GeV}$. Of course if one wants to avoid fine-tuning of the flux superpotential, we would need to take even larger values of \mathcal{V} corresponding to a string scale of 10^{12} GeV . In this case the classical soft terms are completely negligible (for $m_{3/2} \sim 100 \text{ TeV}$) but the (classical) μ -term is also strongly suppressed.

In the rest of this section we will call the holomorphic variable associated with the large modulus τ_b , T .

2.4 Gaugino Masses - Weyl Anomaly Effects

For a generic version of supergravity, the gaugino masses satisfy the following relation at the classical level:

$$\frac{M_a}{g_a^2} = \frac{1}{2} F^A \partial_A f_a(\Phi). \quad (12)$$

For both the single Kähler modulus model and LVS cases, the leading contribution to the gauge coupling function $f_a(\Phi)$ comes from the axio-dilaton S , so at a classical minimum where the SUSY breaking is expected to be in the T modulus direction, the string theoretic contribution to the gaugino mass is highly suppressed.

However, there is an additional contribution to the gaugino mass due to the (super) Weyl anomaly. This comes from the expression for the effective gauge coupling superfield that has been derived by Kaplunovsky and Louis [21] (KL)². For the gaugino masses, the relevant con-

²As explained in [6], the usual formulae for AMSB [5], [20] need modification in the light of [21].

tribution comes from taking the F -term of

$$H_a(\Phi, \tau, \tau_Z) = f_a(\Phi) - \frac{3c_a}{8\pi^2} \ln \phi - \frac{T_a(r)}{4\pi^2} \phi_Z. \quad (13)$$

Here, the first term on the RHS is the classical term; the second comes from the anomaly associated with rotating to the Einstein-Kähler frame. $c_a = T(G_a) - \sum_r T_a(r)$ is the anomaly coefficient and the last term comes from the anomaly associated with the transformation to canonical kinetic terms for the MSSM fields. Also note that we have ignored the gauge kinetic term normalization anomaly [22, 6] which is a higher order effect. The chiral superfields ϕ, ϕ_r that generate these transformations are given by,

$$\ln \phi + \ln \bar{\phi} = \frac{1}{3} K|_{\text{Harm}}, \quad (14)$$

$$\phi_r + \bar{\phi}_r = \ln \det \tilde{K}_{\alpha\beta}^{(r)}. \quad (15)$$

The instruction on the RHS of the first equation is to take the sum of the chiral and anti-chiral (i.e. harmonic) part of the expression. After projecting the appropriate F terms we arrive at the following expression:

$$\frac{2M_a}{g_a^2} = F^A \partial_A f_a - \frac{c_i}{8\pi^2} F^A K_A - \sum_r \frac{T_i(r)}{4\pi^2} F^A \partial_A \ln \det \tilde{K}_{\alpha\beta}^{(r)}. \quad (16)$$

As pointed out earlier, the first (classical) term is greatly suppressed relative to $m_{3/2}$. The dominant contribution therefore comes from the last two (Weyl anomaly) contributions. It turns out that (after using the formulae $F^T = -(T + \bar{T})m_{3/2}$, $K_T = -3/(T + \bar{T})$ and $\tilde{K}_{\alpha\beta} = k_{\alpha\beta}/(T + \bar{T})$ which are valid up to volume suppressed corrections), this yields³,

$$M_a = \frac{b_a g_a^2}{16\pi^2} m_{3/2}, \quad (17)$$

where $b_a = -3T(G_a) + \sum_r T_a(r)$ is the beta function coefficient.

2.5 Scalar Masses, Trilinear Couplings, μ and $B\mu$ terms

Here we summarize the results from this class of string theory models for the values of the soft parameters at the UV scale, *i.e.* $\Lambda \sim M_{string} \sim M_P/\sqrt{\mathcal{V}}$. These values should be the initial conditions for the RG evolution of these parameters. In the LVS case, it was estimated[19] that the lower bound on the CYO volume was $\mathcal{V} > 10^5$. Also, we will choose typical values $h_{21} \sim O(10^2)$ for the number of complex structure moduli. We will also take the gravitino mass $m_{3/2} \sim |W|M_P/\mathcal{V} \sim 50$ TeV. Such a large value of $m_{3/2}$ allows us to avoid the SUGRA gravitino problem, which leads to a disruption of Big Bang nucleosynthesis if $m_{3/2} \lesssim 5$ TeV and $T_R \gtrsim 10^5$ GeV[23].

³Note that we expect the Weyl anomaly expressions for the gaugino masses given below to be valid only because of the particular (extended no-scale) features of this class of string theory models. It so happens that these are exactly the same as the expressions given in what is usually called AMSB: but that is an accident due entirely to the fact that in these extended no-scale models the relationship $F^A K_A \simeq 3m_{3/2}$ is true.

Unlike the gaugino masses, scalar masses and trilinear soft terms do not acquire corrections from the Weyl anomaly. They are essentially given at the UV scale by their classical string theory value plus one loop string/effective field theory corrections. In the $h_{11} = 1$ case, the classical soft terms are essentially zero while in the LVS case

$$m_0 \sim O\left(\frac{m_{3/2}}{\sqrt{\ln m_{3/2}\mathcal{V}}}\right), \mu \sim \frac{B\mu}{\mu} \lesssim \sqrt{h_{21}}m_0, A_0 \ll m_0. \quad (18)$$

After adding quantum corrections at the UV scale both cases give similar values for the soft terms. As an example, we illustrate for two values for the CYO volume:

- $\mathcal{V} \sim 10^5, M_{string} \sim \Lambda \sim 10^{-2.5}M_P \sim 10^{15.5}$ GeV. Then,

$$\mu \sim \frac{B\mu}{\mu} \lesssim 250 \text{ GeV}, m_0 \sim 25 \text{ GeV}, A_0 \ll m_0. \quad (19)$$

- $\mathcal{V} \sim 10^{12}, M_{string} \sim \Lambda \sim 10^{-6}M_P \sim 10^{12}$ GeV. Then,

$$\mu \sim \frac{B\mu}{\mu} \lesssim 10^{-1} \text{ GeV}, m_0 \sim 10^{-2} \text{ GeV}, A_0 \ll m_0. \quad (20)$$

The second very large volume case can be accessed only in the LVS model.

The first case is at the lower bound for the volume. This gives the largest allowable string scale. This is still somewhat below the apparent unification scale, but it is close enough that (allowing for undetermined $O(1)$ factors) we may use the GUT scale as the point at which to impose the boundary conditions. This is useful for the purpose of comparing with other models of SUSY mediation where it is conventional to use the GUT scale.

The second case above corresponds to choosing generic values of the flux superpotential, while the first needs a fine tuned set of fluxes to get $|W| \sim 10^{-8}$, in order to have a gravitino mass of $\sim 10^2$ TeV, though in type IIB string theory general arguments show that there exist a large number of solutions which allow this. The most significant problem with the second case (apart from the fact that there is no hope of getting a GUT scenario) is the extremely low upper bound on the μ term. In other words, there is a serious μ - problem. The first case also may have a μ term problem, but again since these estimates are accurate only to $O(1)$ numbers, it is possible to envisage that the problem can be resolved within the context of this model.

In any case, as we discussed in the introduction, we are going to take an approach where the string theory input is used to suggest a class of phenomenological models. Given that in both the GUT scale model and the intermediate scale model, the soft scalar mass and A term are suppressed well below the weak scale, we will input the value zero for these at the UV scale, while the gaugino masses at this scale are given by (17).

We also discuss the case when the input scalar mass m_0 is non-negligible. This would be the case for instance in the SKM model with smaller volumes and/or larger values of h_{21} , and also in the case of LVS with the volume at the lower bound but with larger values of h_{21} .

3 Mass spectra, parameter space and constraints for the inoAMSB model

3.1 Sparticle mass spectra and parameter space

We begin our discussion by examining the sort of sparticle mass spectra that is expected from the inoAMSB boundary conditions: $m_0 = A_0 = 0$ but with $M_i = \frac{b_i g_i^2}{16\pi^2} m_{3/2}$. We compute the sparticle mass spectra using the Isasugra subprogram of the event generator Isajet[24], along with the option of non-universal gaugino masses. The parameter space is that of Eq. 3.

After input of the above parameter set, Isasugra implements an iterative procedure of solving the MSSM RGEs for the 26 coupled renormalization group equations, taking the weak scale measured gauge couplings and third generation Yukawa couplings as inputs, as well as the above-listed GUT scale SSB terms. Isasugra implements full 2-loop RG running in the \overline{DR} scheme, and minimizes the RG-improved 1-loop effective potential at an optimized scale choice $Q = \sqrt{m_{\tilde{t}_L} m_{\tilde{t}_R}}$ (which accounts for leading two-loop terms)[25] to determine the magnitude of μ and the value of m_A . All physical sparticle masses are computed with complete 1-loop corrections, and 1-loop weak scale threshold corrections are implemented for the t , b and τ Yukawa couplings[26]. The off-set of the weak scale boundary conditions due to threshold corrections (which depend on the entire superparticle mass spectrum), necessitates an iterative up-down RG running solution. The resulting superparticle mass spectrum is typically in close accord with other sparticle spectrum generators[27].

We begin by examining a single point in inoAMSB parameter space, where $m_{3/2} = 50$ TeV, and $\tan\beta = 10$, with $\mu > 0$ as suggested by the $(g-2)_\mu$ anomaly[28, 29]. In Fig. 1, we plot in frame *a*). the running gaugino masses, and in frame *b*). the running third generation and Higgs soft SUSY breaking scalar masses. We actually plot here $sign(m_i^2) \times \sqrt{|m_i^2|}$, in order to show the possible running to negative squared masses, while at the same time showing the true scale of the soft terms in GeV units. Frame *a*). is as expected in most AMSB masses *i.e.* where $M_1 \gg |M_3| \gg M_2$ at $Q = M_{string}$, where here we take $M_{string} = M_{GUT}$. The RG running of the gaugino masses leads to $-M_3 \gg M_1$ at $Q = M_{weak}$, while M_2 remains the lightest of gaugino masses at the weak scale, leading to a wino-like lightest neutralino \tilde{Z}_1 , which might also be the lightest SUSY particle (LSP). In frame *b*)., we see that the SSB scalar masses, beginning with negligible GUT scale values, are initially pulled up to positive values, mainly by the influence of the large value of M_1 at the GUT scale. In fact, the right-slepton mass $m_{E_3}^2$ initially evolves to the highest values, since it has the largest hypercharge quantum number $Y = 2$. The disparate Y values between E_3 and the doublet L_3 lead ultimately to a large splitting between left- and right- slepton SSB masses in the inoAMSB case, while these masses tend to be quite degenerate in mAMSB[30]. As the scale Q moves to values $\ll M_{GUT}$, QCD effects pull the squarks to much higher masses: in this case around the TeV scale, while sleptons, which receive no QCD contribution, remain in the 200-400 GeV range. The value of $m_{H_u}^2$ is driven as usual to negative squared values, resulting in a radiative breakdown of electroweak symmetry (REWSB). Since $M_2 < \sqrt{m_{L_3}^2}$, we generically find a wino-like neutralino as the LSP, and there is no problem with a charged LSP (as in NS/inoMSB models) or tachyonic sleptons (as in AMSB).

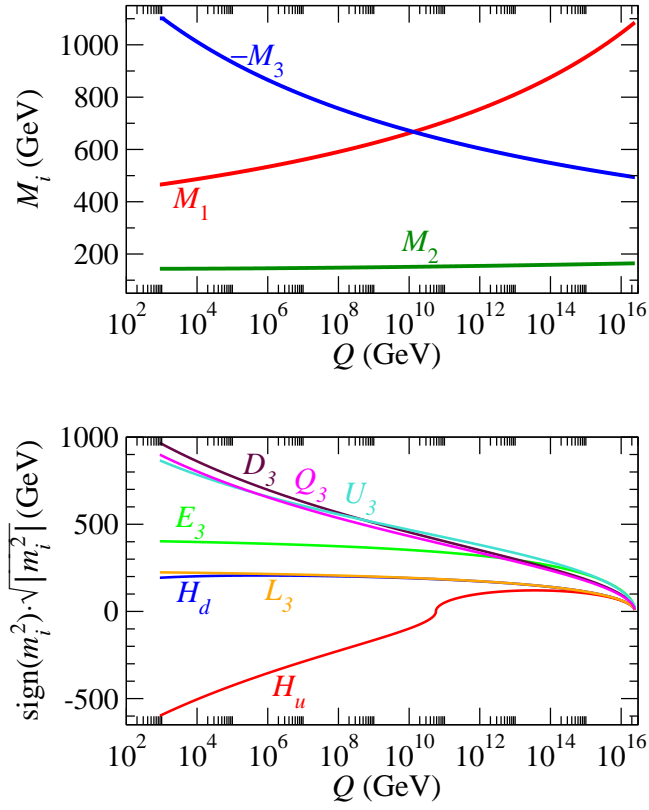


Figure 1: Running of soft SUSY breaking parameters as a function of energy scale Q for $m_{3/2} = 50$ TeV, $\tan\beta = 10$ and $\mu > 0$ in the inoAMSB model, with $M_{string} = M_{GUT}$.

Once the weak scale SSB terms are computed, then the physical mass eigenstates and mixings may be computed, and one-loop mass corrections added. The resulting physical mass spectrum is listed schematically in Fig. 2a). and in Table 1, column 3. We adopt this inoAMSB model as a benchmark case, labeled inoAMSB1. In Table 1, we also show for comparison two related cases with $m_{3/2} = 50$ TeV and $\tan\beta = 10$: for mAMSB supersymmetry in column 1, with $m_0 = 300$ GeV, and in HCAMSB[13], column 2, with mixing parameter $\alpha = 0.025$.⁴ While the first three cases listed in Table 1 have similar values of $m_{\tilde{g}}$ and $m_{\tilde{W}_1, \tilde{Z}_1}$ (due to the same input value of $m_{3/2}$), we see that inoAMSB1 has the previously noted large \tilde{e}_L - \tilde{e}_R splitting, with $m_{\tilde{e}_L} < m_{\tilde{e}_R}$, while mAMSB has nearly degenerate \tilde{e}_L and \tilde{e}_R , with $m_{\tilde{e}_R} < m_{\tilde{e}_L}$. However, the left-right slepton splitting in inoAMSB1 is not as severe as that shown in HCAMSB1, from Ref. [13], where an even larger value of M_1 at M_{GUT} is expected. In the HCAMSB1 case, the \tilde{Z}_4 state tends to be nearly pure bino-like, whereas in inoAMSB1, it is instead higgsino-like.

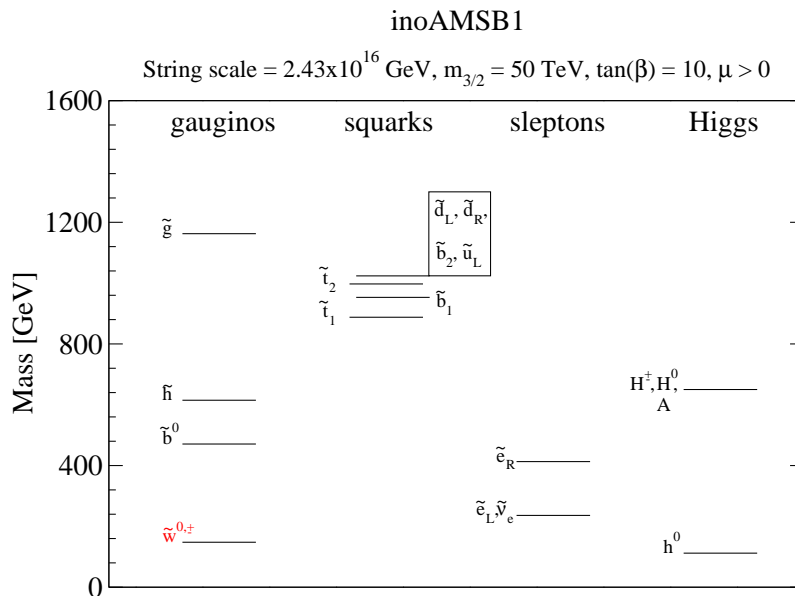


Figure 2: Plot of sparticle masses for the inoAMSB1 case study with $m_{3/2} = 50$ TeV, $\tan\beta = 10$ and $\mu > 0$.

Next, we investigate the effect of varying $m_{3/2}$ on the sparticle mass spectrum. We plot in Fig. 3 the mass spectra of various sparticles versus $m_{3/2}$ in the inoAMSB model while taking $\tan\beta = 10$, $\mu > 0$ and $m_t = 172.6$ GeV. The lowest value of $m_{3/2}$ which is allowed is $m_{3/2} = 32.96$ TeV. Below this value, $m_{\tilde{W}_1} < 91.9$ GeV, which is excluded by LEP2 searches for charginos from AMSB models[31]. We see from Fig. 3 that there is a characteristic mass hierarchy in the inoAMSB model, where $m_{\tilde{Z}_1, \tilde{W}_1} < m_{\tilde{e}_L, \tilde{\nu}_{eL}} < m_{\tilde{e}_R} < |\mu| < m_{\tilde{q}} < m_{\tilde{g}}$. As

⁴In the HCAMSB model, while most of the MSSM resides on a visible brane, $U(1)$ gauginos propagate in the bulk. Thus, the SSB boundary conditions, taken at the GUT scale, are those of AMSB, but with an additional contribution to the hypercharge gaugino mass, proportional to the mixing parameter α .

parameter	mAMSB	HCAMSB1	inoAMSB1	inoAMSB2
α	—	0.025	—	—
m_0	300	—	—	—
$m_{3/2}$	50 TeV	50 TeV	50 TeV	100 TeV
$\tan \beta$	10	10	10	10
M_1	460.3	997.7	465.5	956.1
M_2	140.0	139.5	143.8	287.9
μ	872.8	841.8	607.8	1127.5
$m_{\tilde{g}}$	1109.2	1107.6	1151.0	2186.1
$m_{\tilde{u}_L}$	1078.2	1041.3	1011.7	1908.7
$m_{\tilde{u}_R}$	1086.2	1160.3	1045.1	1975.7
$m_{\tilde{t}_1}$	774.9	840.9	878.8	1691.8
$m_{\tilde{t}_2}$	985.3	983.3	988.4	1814.8
$m_{\tilde{b}_1}$	944.4	902.6	943.9	1779.5
$m_{\tilde{b}_2}$	1076.7	1065.7	1013.7	1908.3
$m_{\tilde{e}_L}$	226.9	326.3	233.7	457.8
$m_{\tilde{e}_R}$	204.6	732.3	408.6	809.5
$m_{\tilde{W}_2}$	879.2	849.4	621.2	1129.8
$m_{\tilde{W}_1}$	143.9	143.5	145.4	299.7
$m_{\tilde{Z}_4}$	878.7	993.7	624.7	1143.2
$m_{\tilde{Z}_3}$	875.3	845.5	614.4	1135.8
$m_{\tilde{Z}_2}$	451.1	839.2	452.6	936.8
$m_{\tilde{Z}_1}$	143.7	143.3	145.1	299.4
m_A	878.1	879.6	642.9	1208.9
m_h	113.8	113.4	112.0	116.0
$\Omega_{\tilde{Z}_1} h^2$	0.0016	0.0015	0.0016	0.007
σ [fb]	7.7×10^3	7.4×10^3	7.5×10^3	439
\tilde{g}, \tilde{q} pairs	15.0%	15.5%	19.1%	3%
EW – ino pairs	79.7%	81.9%	75.6%	93%
slep. pairs	3.7%	0.8%	3.1%	3%
$\tilde{t}_1 \tilde{t}_1$	0.4%	0.2%	0.1%	0%

Table 1: Masses and parameters in GeV units for four case study points mAMSB1, HCAMSB1, inoAMSB1 and inoAMSB2 using Isajet 7.80 with $m_t = 172.6$ GeV and $\mu > 0$. We also list the total tree level particle production cross section in fb at the LHC.

$m_{3/2}$ increases, all these masses grow, but the relative hierarchy is maintained. For such a spectrum with $m_{\tilde{q}} < m_{\tilde{g}}$ and with relatively light sleptons, we would thus expect LHC collider events which are dominated by squark pair production, followed by squark cascade decays $\tilde{q} \rightarrow q\tilde{Z}_i \rightarrow q\tilde{\ell}^\pm\ell^\mp$, which would lead to events with two hard jets (plus additional softer jets) and rich in isolated leptons coming from cascade decay produced sleptons.

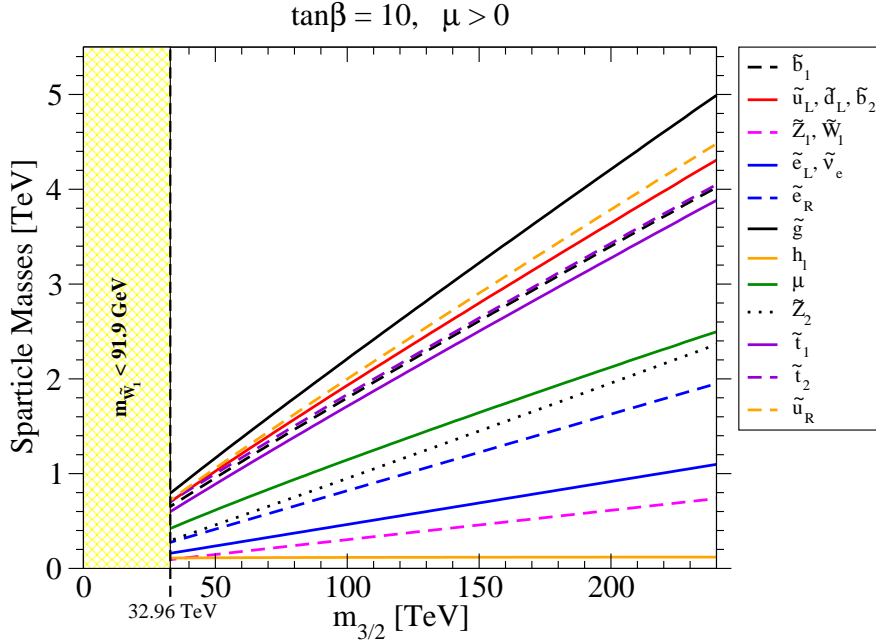


Figure 3: Sparticle mass spectrum versus $m_{3/2}$ in the inoAMSB with $M_{string} = M_{GUT}$, $\tan\beta = 10$, with $\mu > 0$ and $m_t = 172.6$ GeV.

In Fig. 4, we show the variation in sparticle masses against $\tan\beta$ with $m_{3/2}$ fixed at 50 TeV. As $\tan\beta$ increases, the b and τ Yukawa couplings both increase. These act to suppress the sbottom and stau SSB mass terms, and also give larger left-right mixing to the mass eigenstates. In addition, the value of m_A^2 is pushed to negative values by the large b and τ Yukawa couplings. The value of m_A is given approximately from the EWSB minimization conditions as $m_A^2 \sim m_{H_d}^2 - m_{H_u}^2$. Since the mass gap between $m_{H_u}^2$ and $m_{H_d}^2$ drops as $\tan\beta$ increases, the value of m_A also drops sharply with increasing $\tan\beta$. The point at which m_A drops below limits from LEP2 searches (and shortly thereafter REWSB no longer occurs in a valid fashion) provides the high $\tan\beta$ boundary to the parameter space.

In Fig. 5, we show the entire parameter space for the inoAMSB model in the $m_{3/2}$ vs. $\tan\beta$ plane for $\mu > 0$ with $m_t = 172.6$ GeV. The gray shaded region gives allowable sparticle mass spectra. The orange region gives chargino masses below the LEP2 limit, and so is experimentally excluded. The brown shaded region for $\tan\beta \gtrsim 42$ is excluded because REWSB no longer occurs in an appropriate fashion. The brown shaded region at very low $\tan\beta$ gives too light a value of m_h : here we require $m_h > 111$ GeV (even though LEP2 requires $m_h > 114.4$ GeV), due to a projected $\sim \pm 3$ GeV theory error on our lightest Higgs mass calculation. We also show

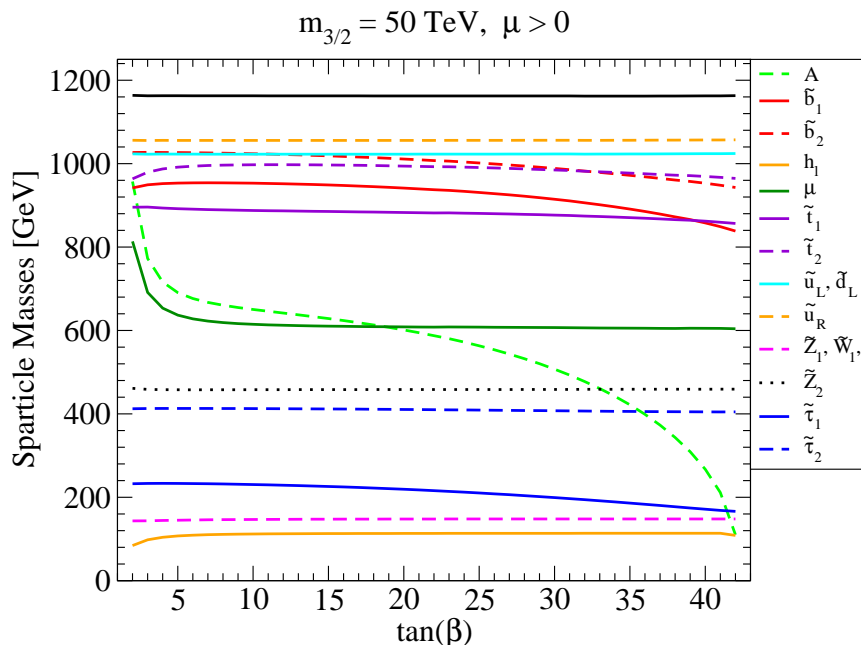


Figure 4: Sparticle mass spectrum versus $\tan\beta$ for $m_{3/2} = 50 \text{ TeV}$ in the inoAMSB with $M_{string} = M_{GUT}$ and with $\mu > 0$.

contours of $m_{\tilde{g}}$ ranging from 1-5 TeV. The $m_{\tilde{g}} \sim 5 \text{ TeV}$ range will surely be beyond the reach of LHC.

As noted in Sec. 2, in the inoAMSB model the string scale M_{string} need not be equal to M_{GUT} . If it is not, then it can have significant effects on the sparticle mass spectrum. The sparticle mass spectrum versus variable M_{string} is shown in Fig. 6 for the case where $m_{3/2} = 50 \text{ TeV}$, $\tan\beta = 10$ and $\mu > 0$. Here, we see that the sparticle mass spectrum spreads out as M_{string} varies from M_{GUT} down to 10^{11} GeV . In addition, some important level crossings occur. Most important of these is that for $M_s \lesssim 5 \times 10^{13} \text{ GeV}$, the $\tilde{\nu}_\tau$ state becomes the lightest MSSM particle, and for even lower M_s values, $m_{\tilde{\nu}_e}$ and $m_{\tilde{\nu}_\mu}$ drop below $m_{\tilde{Z}_1}$. There already exist severe limits on stable sneutrino dark matter[32], which discourage this type of scenario. If we insist upon a neutralino as LSP, then we must take not too low a value of M_s .

Finally, we note that in the inoAMSB model, scalar masses and A -parameters are expected to be suppressed, but they are not expected to be exactly zero. In Fig. 7, we show the mass spectra from inoAMSB models where we add an additional universal mass contribution m_0 to all scalars. We adopt values $m_{3/2} = 50 \text{ TeV}$ and $\tan\beta = 10$ for this plot. As m_0 increases beyond zero, it is seen that the spectra change little so long as $m_0 \lesssim 100 \text{ GeV}$, and also the mass orderings remain intact. For larger values of m_0 , the left- and right- slepton masses begin to increase, with first $m_{\tilde{e}_R}$ surpassing $m_{\tilde{Z}_2}$, and later even $m_{\tilde{e}_L}$ surpasses $m_{\tilde{Z}_2}$. At these high values of m_0 , decay modes such as $\tilde{Z}_2 \rightarrow \ell^\pm \tilde{\ell}^\mp$ would become kinematically closed, thus greatly altering the collider signatures. However, generically in this class of models, we would not

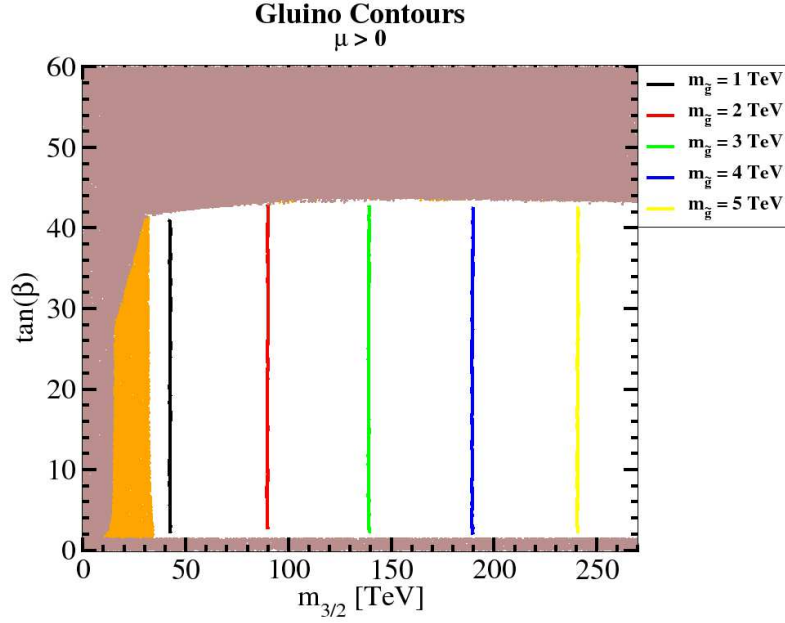


Figure 5: Allowed parameter space of the inoAMSB models in the $m_{3/2}$ vs. $\tan\beta$ plane with $\mu > 0$. We plot also contours of $m_{\tilde{g}}$.

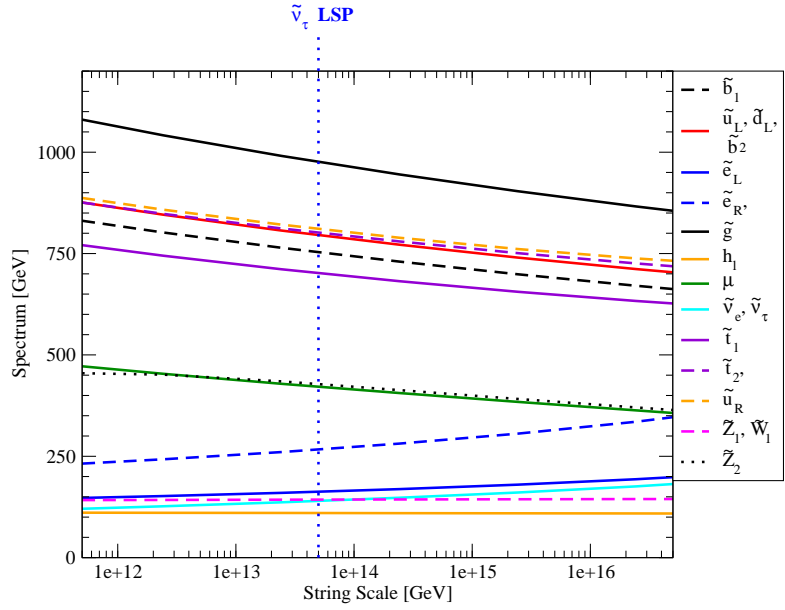


Figure 6: Plot of sparticle masses for the inoAMSB1 case study with $m_{3/2} = 50 \text{ TeV}$, $\tan\beta = 10$ and $\mu > 0$, but with variable value of M_{string} .

expect such large additional contributions to scalar masses.

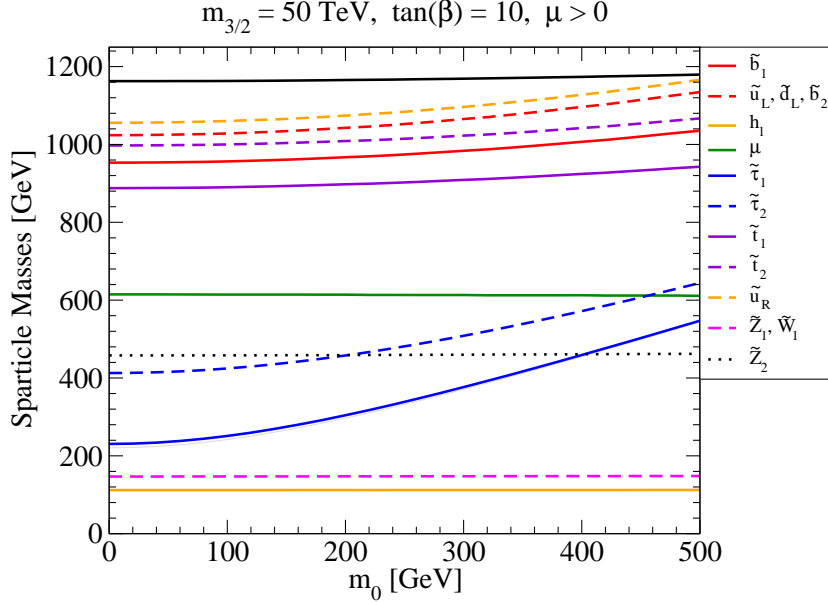


Figure 7: Plot of sparticle masses for the inoAMSB with $m_{3/2} = 50$ TeV, $\tan \beta = 10$ and $\mu > 0$, but with an additional universal contribution m_0 added to all scalar masses.

3.2 $BF(b \rightarrow s\gamma)$ and $(g - 2)_\mu$ in inoAMSB

Along with experimental constraints on the inoAMSB models from LEP2 limits on m_h and $m_{\tilde{W}_1}$, there also exist indirect limits on model parameter space from comparing measured values of $BF(b \rightarrow s\gamma)$ and $\Delta a_\mu \equiv (g - 2)_\mu/2$ against SUSY model predictions.

3.2.1 $BF(b \rightarrow s\gamma)$

As an example, we show in Fig. 8 regions of the branching fraction for $BF(b \rightarrow s\gamma)$ in the inoAMSB model versus $m_{3/2}$ and $\tan \beta$ variation, calculated using the Isatools subroutine ISABSG[33]. The red-shaded region corresponds to branching fraction values within the SM theoretically predicted region $BF(b \rightarrow s\gamma)_{SM} = (3.15 \pm 0.23) \times 10^{-4}$, by a recent evaluation by Misiak[34]. The blue-shaded region corresponds to branching fraction values within the experimentally allowed region[35]: here, the branching fraction $BF(b \rightarrow s\gamma)$ has been measured by the CLEO, Belle and BABAR collaborations; a combined analysis[35] finds the branching fraction to be $BF(b \rightarrow s\gamma) = (3.55 \pm 0.26) \times 10^{-4}$. The gray shaded region gives too large a value of $BF(b \rightarrow s\gamma)$. This region occurs for low $m_{3/2}$, where rather light \tilde{t}_1 and \tilde{W}_1 lead to large branching fractions, or large $\tan \beta$, where also the SUSY loop contributions are enhanced[36].

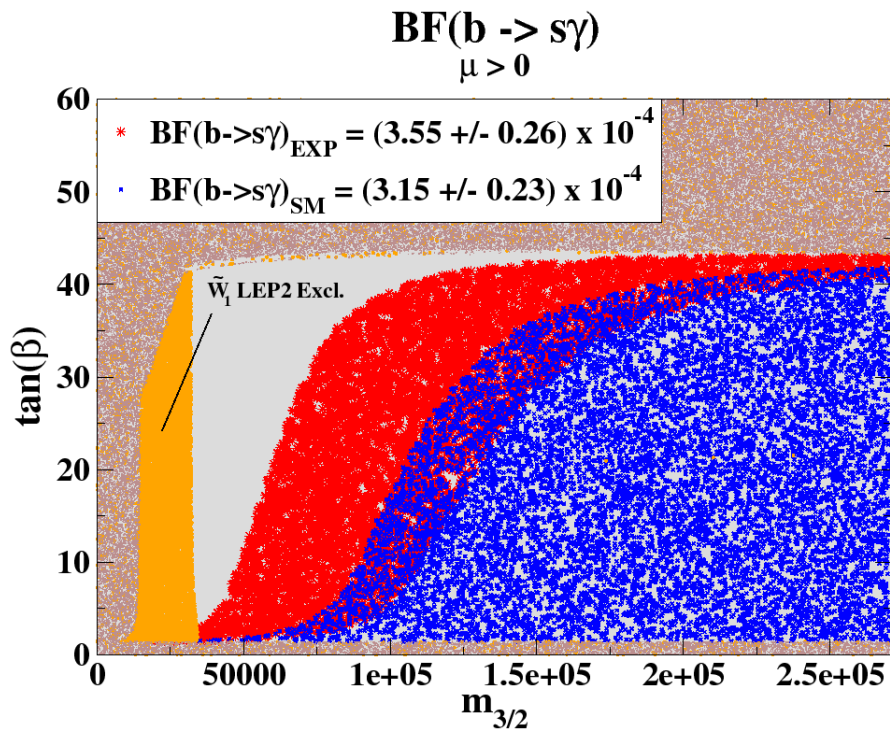


Figure 8: Branching fraction for $b \rightarrow s\gamma$ versus $m_{3/2}$ and $\tan\beta$ variation in the inoAMSB model with $M_{\text{string}} = M_{\text{GUT}}$.

3.2.2 $(g - 2)_\mu/2$

In Fig. 9, we plot the SUSY contribution to Δa_μ : Δa_μ^{SUSY} (using ISAAMU from Isatools[29]). The contribution is large when $m_{3/2}$ is small; in this case, rather light $\tilde{\mu}_L$ and $\tilde{\nu}_{\mu L}$ masses lead to large deviations from the SM prediction. The SUSY contributions to Δa_μ^{SUSY} also increase with $\tan\beta$. It is well-known that there is a discrepancy between the SM predictions for Δa_μ , where τ decay data, used to estimate the hadronic vacuum polarization contribution to Δa_μ , gives rough accord with the SM, while use of $e^+e^- \rightarrow hadrons$ data at very low energy leads to a roughly 3σ discrepancy. The measured Δa_μ anomaly, given as $(4.3 \pm 1.6) \times 10^{-9}$ by the Muon $g - 2$ Collaboration[28], is shown by the black dotted region.

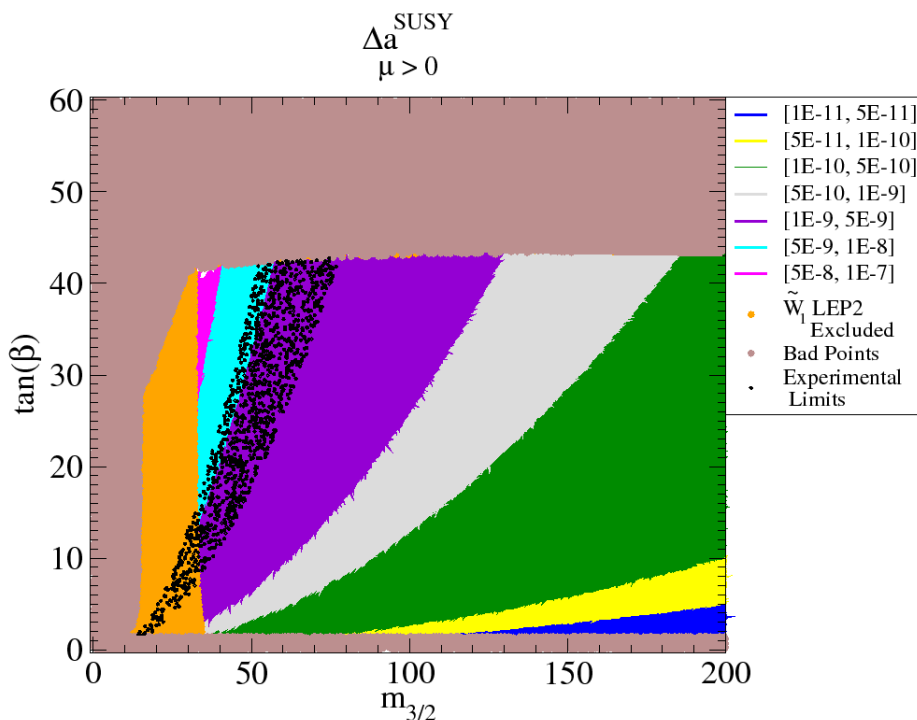


Figure 9: SUSY contribution to Δa_μ versus $m_{3/2}$ and $\tan\beta$ variation in the inoAMSB model with $M_{string} = M_{GUT}$. We also take $\mu > 0$ and $m_t = 172.6$ GeV.

3.2.3 Dark matter in inoAMSB

Finally, we remark upon the relic density of dark matter in the inoAMSB model. If thermal production of the lightest neutralino is assumed to give the dominant DM in the universe, then all over parameter space, the predicted neutralino abundance $\Omega_{\tilde{Z}_1} h^2$ is far below the WMAP measured value of $\Omega_{CDM} h^2 \sim 0.11$. Some sample calculated values are listed in Table 1. It has been suggested in Ref. [37] that production and decay of moduli fields or other processes can also contribute to the DM abundance. Decay of moduli fields in the early universe could then

account for the discrepancy between the measured DM abundance and the predicted thermal abundance in inoAMSB models.

As an alternative, if the strong CP problem is solved via the Peccei-Quinn mechanism, then a superfield containing the axion/axino multiplet should occur. In this case, a mixture of axions[38] and axinos[39], rather than wino-like neutralinos, could constitute the DM abundance[40]. The exact abundance will depend on the axino mass $m_{\tilde{a}}$, the Peccei-Quinn breaking scale f_a , and the re-heat temperature T_R after inflation.

In light of these two alternative DM mechanisms, we regard the inoAMSB parameter space as essentially unconstrained by the measured abundance of DM in the universe.

4 The inoAMSB model and the LHC

4.1 Sparticle production at LHC

In the inoAMSB model, for benchmark point inoAMSB1, we list several sparticle production cross sections in Table 1. We see that for this case, the dominant sparticle production consists of electroweak-ino pair production: mainly $pp \rightarrow \tilde{W}_1^+ \tilde{W}_1^-$ and $\tilde{W}_1^\pm \tilde{Z}_1$ reactions. Since \tilde{Z}_1 is stable (or quasi-stable in the event of light axino dark matter), and mainly $\tilde{W}_1^\pm \rightarrow \pi^\pm \tilde{Z}_1$ (where the π^\pm is very soft), these reactions do not provide enough visible energy to meet detector trigger requirements (unless there is substantial initial state radiation).

The major visible production reactions consist of $pp \rightarrow \tilde{g}\tilde{g}$, $\tilde{g}\tilde{q}$ and $\tilde{q}\tilde{q}$ production (here, we take \tilde{q} to represent generic species of both squarks and anti-squarks). In the case of inoAMSB models, we expect $m_{\tilde{q}} \sim 0.9m_{\tilde{g}}$. Strongly interacting sparticle production cross sections (at NLO using Prospino[41]) are shown versus $m_{3/2}$ in Fig. 10 for $\tan\beta = 10$, $\mu > 0$ and $M_s = M_{GUT}$. We see that the reactions $pp \rightarrow \tilde{q}\tilde{q}$ and $\tilde{q}\tilde{g}$ are roughly comparable, with $\tilde{q}\tilde{g}$ production dominating for $m_{3/2} \lesssim 65$ TeV, and $\tilde{q}\tilde{q}$ pair production dominating for higher $m_{3/2}$ values. The $pp \rightarrow \tilde{g}\tilde{g}$ production cross section always occurs at much lower rates. For $m_{\tilde{g}} \sim 3$ TeV, corresponding to $m_{3/2} \sim 150$ TeV, the total hadronic SUSY cross section is around 0.1 fb, which should be around the upper limit of LHC reach given 100 fb⁻¹ of integrated luminosity.

Since sleptons are much lighter than squarks in inoAMSB models, we also expect possibly observable rates for slepton pair production. Pair production rates for $pp \rightarrow \tilde{e}_L^+ \tilde{e}_L^-$, $\tilde{e}_R^+ \tilde{e}_R^-$ and $\tilde{\nu}_{eL} \tilde{e}_L$ are also shown in Fig. 10. Typically, the LHC reach for direct slepton pair production ranges up to $m_{\tilde{e}} \sim 350$ GeV for 10 fb⁻¹[42], corresponding to a $m_{3/2}$ value of ~ 75 TeV. Thus, LHC reach should be much higher in the hadronic SUSY production channels.

4.2 Sparticle decays in inoAMSB models

Since $m_{\tilde{g}} > m_{\tilde{q}}$ in inoAMSB models, we will have $\tilde{g} \rightarrow q\tilde{q}$, nearly democratically to all squark species. The left-squarks will dominantly decay to *wino* + q , and we find $\tilde{q}_L \rightarrow q\tilde{W}_1$ at $\sim 67\%$, while $\tilde{q}_L \rightarrow q\tilde{Z}_1$ at $\sim 33\%$, all over parameter space. The right-squark decays are simpler. The \tilde{q}_R decays mainly to *bino* + q , so that in the inoAMSB model line, we obtain $\tilde{q}_R \rightarrow \tilde{Z}_2 q$ at $\sim 97\%$ over almost all parameter space, since in this case \tilde{Z}_2 is nearly pure bino-like.

For the sleptons, the left-sleptons dominantly decay to *wino* + *lepton*, so we find $\tilde{\ell}_L \rightarrow \ell\tilde{Z}_1$ at $\sim 33\%$, and $\tilde{\ell}_L \rightarrow \tilde{W}_1 \nu_{\ell L}$ at $\sim 67\%$ all over parameter space. The latter decay mode should

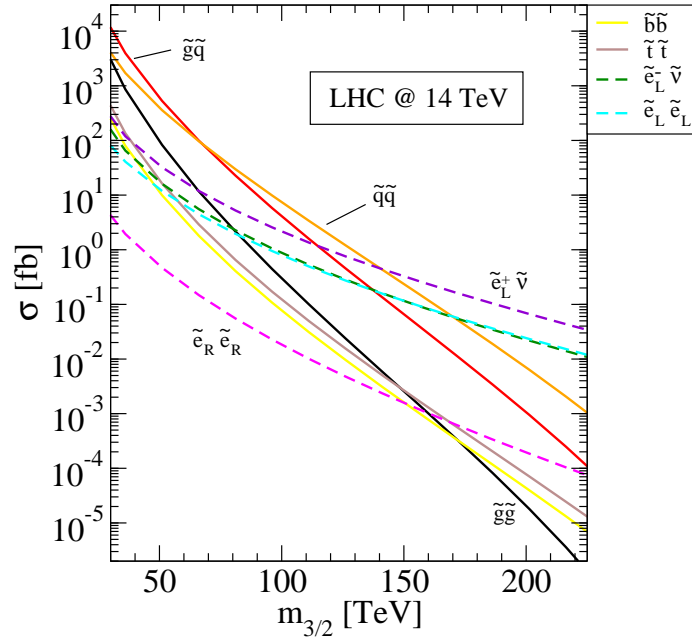


Figure 10: Sparticle pair production cross sections at LHC with $\sqrt{s} = 14$ TeV for the inoAMSB model with $\tan\beta = 10$ and $\mu > 0$.

be nearly invisible, unless the highly ionizing \widetilde{W}_1 track is found in the micro-vertex detector. The sneutrino decays as $\tilde{\nu}_{\ell L} \rightarrow \tilde{Z}_1 \nu_{\ell}$ at $\sim 33\%$, which is again nearly invisible. However, it also decays via $\tilde{\nu}_{\ell L} \rightarrow \ell \widetilde{W}_1$ at $\sim 66\%$, which provides a detectable decay mode for the sneutrinos. The \tilde{e}_R would like to decay to *bino* + *lepton*, but in the case of inoAMSB models, the bino-like neutralino is too heavy for this decay to occur. In the case of inoAMSB1 benchmark point, we instead get $\tilde{\ell}_R \rightarrow e \tilde{Z}_1$ at $\sim 78\%$. Since this decay mode is suppressed, some three body decay modes can become comparable. In his case, we find $\tilde{\ell}_R^- \rightarrow \ell^- \tau^+ \tilde{\tau}_1^-$ at $\sim 13\%$, and $\tilde{\ell}_R^- \rightarrow \ell^- \tau^- \tilde{\tau}_1^+$ at $\sim 7\%$.

4.3 LHC collider events for the inoAMSB models

We use Isajet 7.80[24] for the simulation of signal and background events at the LHC. A toy detector simulation is employed with calorimeter cell size $\Delta\eta \times \Delta\phi = 0.05 \times 0.05$ and $-5 < \eta < 5$. The hadronic calorimeter (HCAL) energy resolution is taken to be $80\%/\sqrt{E} + 3\%$ for $|\eta| < 2.6$ and forward calorimeter (FCAL) is $100\%/\sqrt{E} + 5\%$ for $|\eta| > 2.6$. The electromagnetic (ECAL) energy resolution is assumed to be $3\%/\sqrt{E} + 0.5\%$. We use the UA1-like jet finding algorithm GETJET with jet cone size $R = 0.4$ and require that $E_T(\text{jet}) > 50$ GeV and $|\eta(\text{jet})| < 3.0$. Leptons are considered isolated if they have $p_T(e \text{ or } \mu) > 20$ GeV and $|\eta| < 2.5$ with visible activity within a cone of $\Delta R < 0.2$ of $\Sigma E_T^{\text{cells}} < 5$ GeV. The strict isolation criterion helps reduce multi-lepton backgrounds from heavy quark ($c\bar{c}$ and $b\bar{b}$) production.

We identify a hadronic cluster with $E_T > 50$ GeV and $|\eta(j)| < 1.5$ as a *b*-jet if it contains a *B* hadron with $p_T(B) > 15$ GeV and $|\eta(B)| < 3$ within a cone of $\Delta R < 0.5$ about the jet axis. We adopt a *b*-jet tagging efficiency of 60%, and assume that light quark and gluon jets can be mis-tagged as *b*-jets with a probability 1/150 for $E_T < 100$ GeV, 1/50 for $E_T > 250$ GeV, with a linear interpolation for $100 \text{ GeV} < E_T < 250 \text{ GeV}$ [43].

We have generated 2M events for case inoAMSB1 from Table 1. In addition, we have generated background events using Isajet for QCD jet production (jet-types include g, u, d, s, c and b quarks) over five p_T ranges as shown in Table 2. Additional jets are generated via parton showering from the initial and final state hard scattering subprocesses. We have also generated backgrounds in the $W + \text{jets}$, $Z + \text{jets}$, $t\bar{t}(172.6)$ and WW, WZ, ZZ channels at the rates shown in the same Table. The $W + \text{jets}$ and $Z + \text{jets}$ backgrounds use exact matrix elements for one parton emission, but rely on the parton shower for subsequent emissions.

For our initial selection of signal events, we first require the following minimal set of cuts labeled **C1**:

- $n(\text{jets}) \geq 2$,
- $E_T^{\text{miss}} > \max(100 \text{ GeV}, 0.2M_{\text{eff}})$
- $E_T(j1, j2) > 100, 50 \text{ GeV}$,
- transverse sphericity $S_T > 0.2$,

where $M_{\text{eff}} = E_T^{\text{miss}} + E_T(j1) + E_T(j2) + E_T(j3) + E_T(j4)$.

Since sparticle production in inoAMSB models is dominated by $\tilde{q}\tilde{g}$ and $\tilde{q}\tilde{q}$ reactions, followed by $\tilde{q} \rightarrow q\tilde{Z}_i$ or $q'\tilde{W}_j$, we expect at least two very hard jets in each signal event. In Fig. 11,

we plot out the distribution in $a)$. hardest and $b)$. second hardest jet p_T for the signal case inoAMSB1 along with the summed SM background (denoted by gray histograms). In the case of $p_T(j_1)$, background is dominant for lower p_T values $\lesssim 400$ GeV, while signal emerges from background for higher p_T values. In the case of $p_T(j_2)$, signal emerges from background already around 250-300 GeV. The rather hard jet p_T distributions are characteristic of squark pair production, followed by 2-body squark decay into a hard jet.

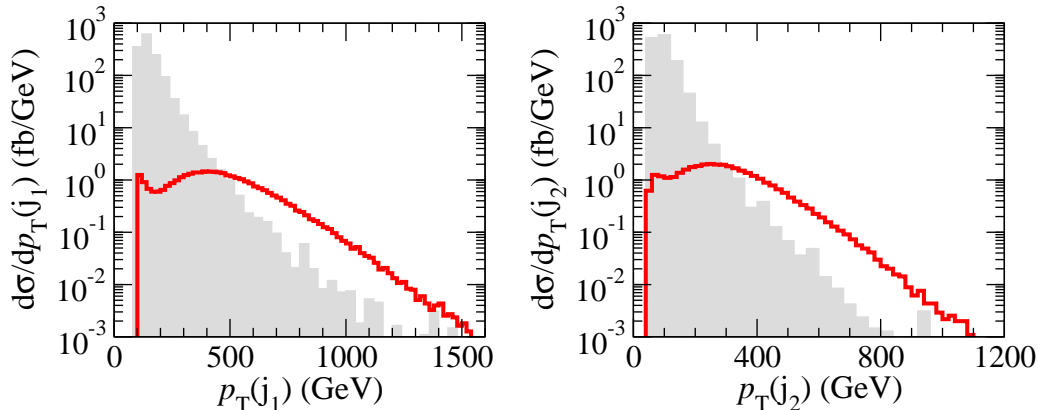


Figure 11: Distribution in p_T of $a)$. the hardest and $b)$. second hardest jets from the inoAMSB1 model, and summed SM background (gray histogram), for LHC collisions at $\sqrt{s} = 14$ TeV.

In Fig. 12, we show the distributions in $a)$. E_T^{miss} and $b)$. $A_T = \sum E_T$ (where the sum extends over all jets and isolated leptons) expected from inoAMSB1 along with SM background. In this case, the E_T^{miss} distribution from SUSY emerges from background at around 400-500 GeV, illustrating the rather hard E_T^{miss} distribution expected from $\tilde{g}\tilde{g}$ and $\tilde{q}\tilde{q}$ pair production, followed by 2-body decays. The A_T signal distribution actually exhibits two components: a soft peak around 400 GeV which comes from chargino, neutralino and slepton pair production, and a hard peak at much higher values coming from gluino and squark pair production. The low peak is buried under background, while the higher peak emerges from background at around 1400 GeV.

Fig. 13 shows the distribution in $a)$. jet multiplicity n_j and $b)$. isolated lepton (both e s and μ s) multiplicity n_ℓ from the inoAMSB1 benchmark, compared to SM background after C1 cuts. While the signal is dominated by $\tilde{q}\tilde{q}$ and $\tilde{q}\tilde{g}$ pair production, the jet multiplicity actually exhibits a broad peak around $n_j \sim 2 - 5$. Nominally, we would expect dijet dominance from squark pair production. But additional jets from cascade decays and initial state radiation help broaden the distribution. The broadness of the distribution also depends on our jet E_T cut, which requires only that $E_T(\text{jet}) > 50$ GeV. In the case of isolated lepton multiplicity, we see that background dominates signal for $n_\ell = 0, 1$ and 2 . However, BG drops more precipitously as n_ℓ increases, so that for $n_\ell = 3$ or 4 , signal now dominates background[44]. In these cases, even with minimal cuts, an isolated $3\ell + \geq 2 \text{ jets} + E_T^{\text{miss}}$ signal should stand out well above background.

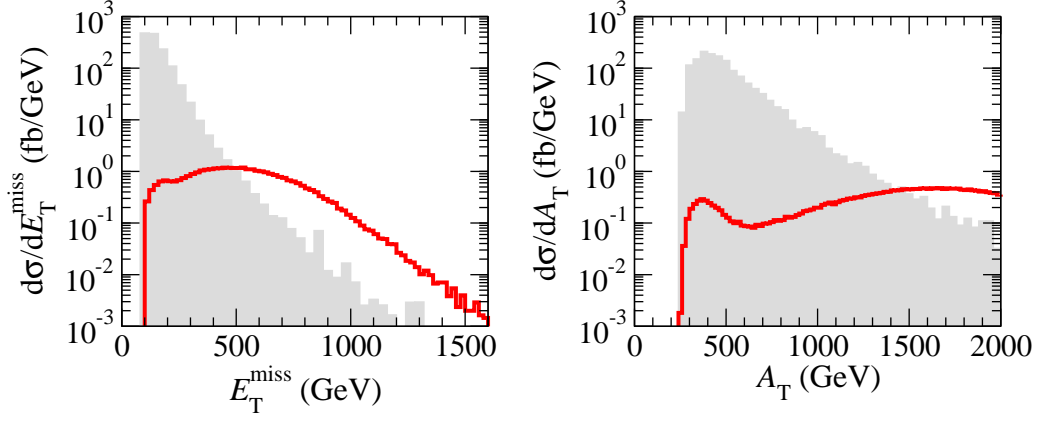


Figure 12: Distribution in *a*). E_T^{miss} and *b*). A_T from the inoAMSB1 model, and summed SM background (gray histogram), for LHC collisions at $\sqrt{s} = 14$ TeV.

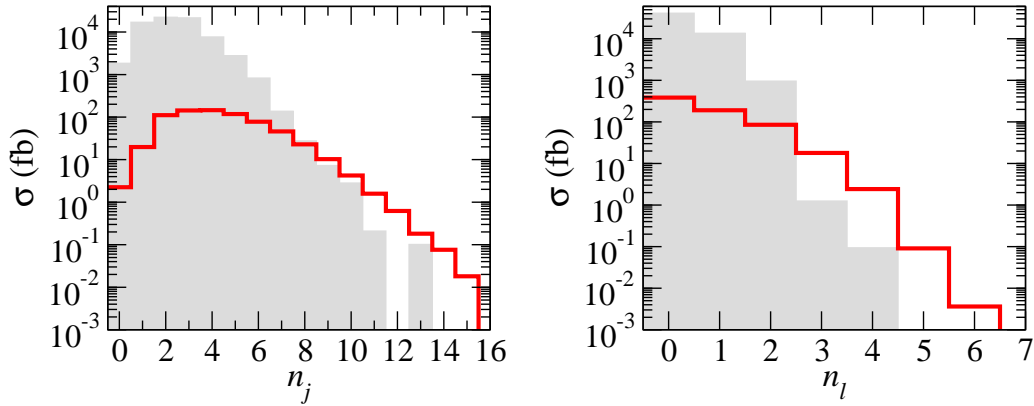


Figure 13: Distribution in *a*). $n(\text{jets})$ and *b*). $n(\text{leptons})$ from the inoAMSB1 model, and summed SM background (gray histogram), for LHC collisions at $\sqrt{s} = 14$ TeV.

4.3.1 LHC cascade decay events including HITs: a smoking gun for models with wino-like neutralinos

Of course, a distinctive property of models like inoAMSB (and also mAMSB and HCAMSB) with a wino-like \tilde{Z}_1 state is that the chargino is very long lived[45]: of order $\sim 10^{-10}$ sec. Thus, once we have obtained cascade decay signal events in any of the multi-jet plus multi-lepton plus E_T^{miss} channels, we may in addition look for the presence of a highly-ionizing track (HIT) from the long-lived chargino. The presence of HITs in the SUSY collider events would be indictative of models such as inoAMSB, mAMSB or HCAMSB, where $M_2 \ll M_1$ and M_3 , so that the lightest neutralino is a nearly pure wino state and where $m_{\tilde{W}_1} \simeq m_{\tilde{Z}_1}$.

4.4 The reach of LHC in the inoAMSB model line

We would next like to investigate the reach of the CERN LHC for SUSY in the inoAMSB context. To this end, we will adopt the inoAMSB model line with variable $m_{3/2}$ but fixed $\tan\beta = 10$ and $\mu > 0$. The sparticle mass spectra versus $m_{3/2}$ was shown previously in Fig. 3

Motivated by the previous signal and background distributions, we will require the following cuts $C2$ [46]:

- $n(\text{jets}) \geq 2$
- $S_T > 0.2$
- $E_T(j1), E_T(j2), E_T^{\text{miss}} > E_T^c$,

where E_T^c can be variable. Parameter space points with lower sparticle masses will benefit from lower choices of E_T^c , while points with heavier sparticle masses– with lower cross sections but higher energy release per event– will benefit from higher choices of E_T^c . In addition, in the zero-leptons channel we require $30^\circ < \Delta\phi(\vec{E}_T^{\text{miss}}, \vec{E}_T(j_c)) < 90^\circ$ between the \vec{E}_T^{miss} and the nearest jet in transverse opening angle. For all isolated leptons ℓ , we require $p_T(\ell) > 20$ GeV. We separate the signal event channels according to the multiplicity of isolated leptons: we exhibit the 0ℓ , opposite-sign (OS) dilepton, 3ℓ and 4ℓ channels. Here, we do not here require “same flavor” on the OS dilepton events. We suppress the 1ℓ and same-sign dilepton SS channels for brevity, and because the reach is better in the channels shown.

The resultant cross sections after cuts $C2$ for SM backgrounds along with signal point inoAMSB1 are listed in Table 2 for $E_T^c = 100$ GeV. For each BG channel, we have generated ~ 2 million simulated events. With the hard cuts $C2$, we are unable to pick up BG cross sections in some of the multi-lepton channels. We will consider a signal to be observable at an assumed value of integrated luminosity if *i*) the signal to background ratio, $S/BG \geq 0.1$, *ii*) the signal has a minimum of five events, and *iii*) the signal satisfies a statistical criterion $S \geq 5\sqrt{BG}$ (a 5σ effect).

Using the above criteria, the 100 fb^{-1} reach of the LHC can be computed for each signal channel. In Fig. 14, we show the signal rates versus $m_{3/2}$ for the inoAMSB model line for $E_T^c = 100$ (solid blue), 300 (dot-dash red) and 500 GeV (dashed purple). The 100 fb^{-1} LHC reach is denoted by the horizontal lines for each E_T^c value. From frame *a*)., for the multi-jet+ E_T^{miss} + 0ℓ signal, we see the LHC reach in the 0ℓ channel extends to $m_{3/2} \sim 40, 93$ and

process	0ℓ	OS	SS	3ℓ	4ℓ
QCD(p_T : 0.05-0.10 TeV)	–	–	–	–	–
QCD(p_T : 0.10-0.20 TeV)	755.1	–	–	–	–
QCD(p_T : 0.20-0.40 TeV)	803.8	621.1	109.6	36.5	–
QCD(p_T : 0.40-1.00 TeV)	209.8	304.7	72.6	29.0	2.6
QCD(p_T : 1.00-2.40 TeV)	2.2	5.3	1.7	1.5	0.2
$t\bar{t}$	1721.4	732.6	273.8	113.3	6.6
$W + jets; W \rightarrow e, \mu, \tau$	527.4	22.6	8.4	1.3	–
$Z + jets; Z \rightarrow \tau\bar{\tau}, \nu s$	752.9	11.1	1.3	0.2	–
WW, ZZ, WZ	3.4	0.3	0.25	–	–
<i>summed SM BG</i>	4776.1	1697.8	467.7	181.9	9.4
inoAMSB1	112.7	85.7	27.6	36.0	7.5

Table 2: Estimated SM background cross sections (plus the inoAMSB1 benchmark point) in fb for various multi-lepton plus jets $+E_T^{\text{miss}}$ topologies after cuts C2 with $E_T^c = 100$ GeV.

E_T^c (GeV)	0ℓ	OS	3ℓ	4ℓ
100	40	57	60	75
300	93	95	98	80
500	110	115	118	110

Table 3: Estimated reach of 100 fb⁻¹ LHC for $m_{3/2}$ (TeV) in the inoAMSB model line in various signal channels.

110 TeV for $E_T^c = 100, 300$ and 500 GeV, respectively, for the inoAMSB model line. This corresponds to a reach in $m_{\tilde{g}}$ of 1.1, 2.0 and 2.4 TeV.

Frames *b)*, *c)* and *d)* show the reach in the multi-jet+ E_T^{miss} + OS , 3ℓ and 4ℓ channels, respectively. While the reach is qualitatively similar in all channels, the best reach comes from the 3ℓ channel, where the 100 fb⁻¹ LHC can detect inoAMSB models up to $m_{3/2} \sim 118$ TeV (corresponding to a reach in $m_{\tilde{g}}$ of 2.6 TeV), using $E_T^c = 500$ GeV. The 100 fb⁻¹ LHC reach for all cases is summarized in Table 3.

4.4.1 Cascade decays including HITs plus a multi-bump $m(\ell^+\ell^-)$ distribution: a smoking gun for inoAMSB models

Next, we examine the distribution in $m(\ell^+\ell^-)$ for cascade decay events containing: ≥ 2 high p_T jets, large E_T^{miss} and a pair of same flavor/opposite-sign (SF/OS) dileptons. This distribution has for long been touted as being very useful as a starting point for reconstructing sparticle masses in SUSY cascade decay events, because it may contain a kinematic mass edge from $\tilde{Z}_2 \rightarrow \tilde{\ell}^\pm \ell^\mp$ or $\tilde{Z}_2 \rightarrow \ell^+ \ell^- \tilde{Z}_1$ decays. In the case of the inoAMSB1 benchmark model, where $m_{\tilde{\ell}_{L,R}} < m_{\tilde{Z}_2}$ and a substantial mass gap between $m_{\tilde{\ell}_L}$ and $m_{\tilde{\ell}_R}$ is featured– we expect *two* distinct, well-separated mass edges: one from $\tilde{Z}_2 \rightarrow \tilde{\ell}_L \ell$ and one from $\tilde{Z}_2 \rightarrow \tilde{\ell}_R \ell$ decays. In addition, a peak at $m(\ell^+\ell^-) \sim M_Z$ is expected, since real Z bosons can be emitted from

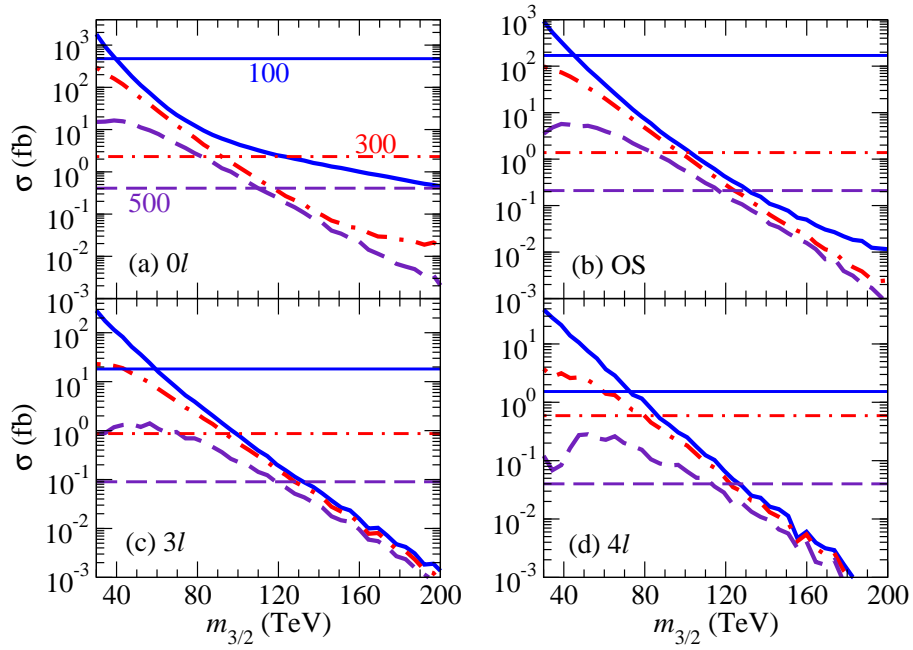


Figure 14: Cross section for multi-jet plus E_T^{miss} events with *a*). $n(\ell) = 0$, *b*). OS isolated dileptons *c*). isolated 3ℓ s and *d*). isolated 4ℓ s at the LHC after cuts $C2$ listed in the text with $E_T^c = 100$ GeV (blue solid), $E_T^c = 300$ GeV (red dot-dashed) and $E_T^c = 500$ GeV (purple dashes), versus $m_{3/2}$, from the inoAMSB model line points with $\tan\beta = 10$ and $\mu > 0$. We also list the $100 \text{ fb}^{-1} 5\sigma$, 5 event, $S > 0.1$ BG limit with the horizontal lines.

cascade decays including $\tilde{Z}_3 \rightarrow Z\tilde{Z}_1$, $\tilde{Z}_4 \rightarrow Z\tilde{Z}_1$ and $\tilde{W}_2 \rightarrow Z\tilde{W}_1$ (in the case of benchmark model inoAMSB1, these decays occur with branching fractions 25%, 6% and 29%, respectively).

In Fig. 15, we show the $m(\ell^+\ell^-)$ distribution from inoAMSB1 (red histogram) in frame *a*). Here, we require cuts $C1$, along with $E_T^{\text{miss}} > 300$ GeV and $A_T > 900$ GeV, which completely suppresses SM backgrounds. Indeed, we see clearly a Z boson peak at M_Z , along with two

distinct mass edges occurring at $m(\ell^+\ell^-) = m_{\tilde{Z}_2} \sqrt{1 - \frac{m_{\tilde{\ell}}^2}{m_{\tilde{Z}_2}^2}} \sqrt{1 - \frac{m_{\tilde{Z}_1}^2}{m_{\tilde{\ell}}^2}} = 182$ GeV, and 304 GeV.

The 182 GeV edge comes from \tilde{Z}_2 decays through $\tilde{\ell}_R$, while the 304 GeV edge comes from \tilde{Z}_2 decays through $\tilde{\ell}_L$. We also show the same distribution for the mAMSB1 (green) and HCAMSB1 (blue) cases from Table 1. The mAMSB plot contains two mass edges as well. However, since in mAMSB we expect $m_{\tilde{\ell}_L} \simeq m_{\tilde{\ell}_R}$, these edges nearly overlap, and are essentially indistinguishable. In the case of HCAMSB models, the bino-like neutralino is the \tilde{Z}_4 and is quite heavy, while \tilde{Z}_2 and \tilde{Z}_3 are mainly higgsino-like. The higgsino-like states decay strongly to vector bosons, as does \tilde{W}_2 , giving rise to a continuum $m(\ell^+\ell^-)$ distribution which contains a Z peak[13]. Thus, while the presence of SUSY cascade decay events at LHC containing HITs would point to AMSB-like models, the different $m(\ell^+\ell^-)$ distributions which are expected would allow one to differentiate between the mAMSB, HCAMSB and inoAMSB cases!

In frame *b*)., we show inoAMSB models with $m_{3/2} = 70$ and 80 GeV. These distributions also show the expected double edge plus Z peak structure that was found for inoAMSB1, although now the mass edges have migrated to higher $m(\ell^+\ell^-)$ values.

5 Discussion and conclusions

In this paper, we have examined the phenomenology of supersymmetric models with the boundary conditions $m_0 \sim A_0 \sim 0$ at M_{GUT} , while gaugino masses assume the form as given in AMSB. We call this model gaugino-AMSB, or inoAMSB or short. Such boundary conditions can arise in type IIB string models with flux compactifications. They are very compelling in that off-diagonal flavor violating and also CP violating terms are highly suppressed, as in the case of no-scale supergravity or gaugino-mediated SUSY breaking models. However, since gaugino masses assume the AMSB form at M_{GUT} , the large $U(1)_Y$ gaugino mass M_1 pulls slepton masses to large enough values through renormalization group evolution that one avoids charged LSPs (as in NS or inoMSB model) or tachyonic sleptons (as in pure AMSB models).

The expected sparticle mass spectrum is very distinctive. Like mAMSB and HCAMSB, we expect a wino-like lightest neutralino \tilde{Z}_1 , and a quasi-stable chargino \tilde{W}_1 which could leave observable highly ionizing tracks in a collider detector. The spectrum is unlike mAMSB in that a large mass splitting is expected between left- and right- sleptons. We also investigated what happens if the string scale M_s is much lower than M_{GUT} . In this case, the entire spectrum become somewhat expanded, and if $M_s \lesssim 10^{14}$ GeV, then the left-sneutrino becomes the LSP, which is excluded by double beta decay experiments.

We also investigated in detail some aspects of LHC collider signatures. Since $m_{\tilde{q}} < m_{\tilde{g}}$ in inoAMSB models, we expect dominant $\tilde{q}\tilde{q}$ and $\tilde{q}\tilde{g}$ production at LHC, followed by 2-body \tilde{q} and \tilde{g} decays. This leads to collider events containing at least two very high p_T jets plus E_T^{miss} as is indicative from squark pair production.

$$n_j \geq 2, E_{j_1}^T > 100, E_{j_2}^T > 50, E_{miss}^T > \max(300, .2M_{eff}),$$

$$A_T > 900, S_T > .2$$

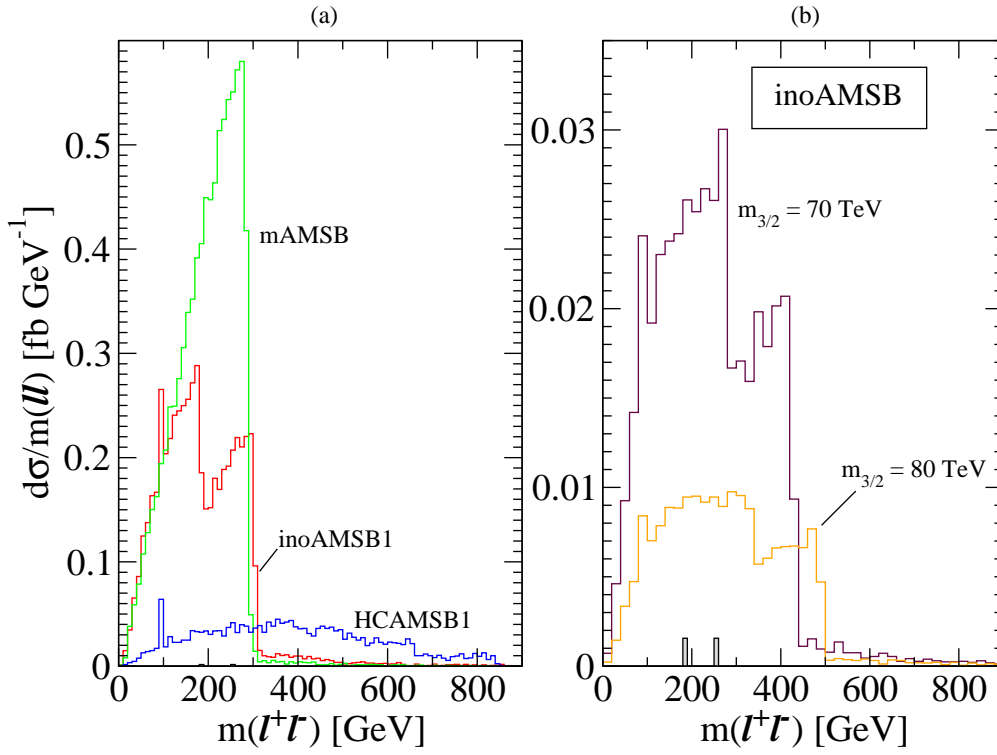


Figure 15: Invariant mass distribution for SF/OS dileptons from *a*). mAMS B1, HCAMS B1 and inoAMS B1 after requiring cut set $C1$ plus $E_T^{miss} > 300$ GeV and $A_T > 900$ GeV. In frame *b*), we show the same distribution, except taking inoAMS B with $m_{3/2} = 70$ and 80 TeV.

While squark and gluino cascade decay events should be easily seen at LHC (provided $m_{3/2} \gtrsim 110$ TeV), the signal events should all contain visible HITS, which would point to a model with $m_{\tilde{W}_1} \simeq m_{\tilde{Z}_1}$, as occurs in anomaly-mediation where $M_2 < M_1, M_3$ at the weak scale. We find an LHC reach for 100 fb^{-1} of integrated luminosity out to $m_{3/2} \sim 118$ TeV, corresponding to a reach in $m_{\tilde{g}}$ of about 2.6 TeV.

We also find that the invariant mass distribution of SF/OS dilepton pairs should have a distinctive two-bump structure that is indicative of neutralino decays through both left- and right- sleptons with a large slepton mass splitting. This distribution would help distinguish inoAMSB models from HCAMSB, where a continuum plus a Z -bump distribution is expected, or from mAMSB, where the two mass edges (present only if m_0 is small enough that $m_{\tilde{\ell}_L}$ and $m_{\tilde{\ell}_R}$ are lighter than $m_{\tilde{Z}_2}$) would be very close together, and probably not resolvable.

Acknowledgments

This work was supported in part by the U.S. Department of Energy. SdA and KG are supported in part by the United States Department of Energy under grant DE-FG02-91-ER-40672.

References

- [1] M. Grana, *Phys. Rept.* **423**, 91 (2006) [arXiv:hep-th/0509003].
- [2] M. R. Douglas and S. Kachru, *Rev. Mod. Phys.* **79**, 733 (2007) [arXiv:hep-th/0610102].
- [3] S. Kachru, R. Kallosh, A. Linde and S. Trivedi, *Phys. Rev. D* **68** (2003) 046005.
- [4] V. Balasubramanian, P. Berglund, J. P. Conlon and F. Quevedo, *J. High Energy Phys.* **03** (2005) 007.
- [5] L. Randall and R. Sundrum, *Nucl. Phys. B* **557** (1999) 79; G. Giudice, M. Luty, H. Murayama and R. Rattazzi, *J. High Energy Phys.* **12** (1998) 027.
- [6] S. P. de Alwis, *Phys. Rev. D* **77** (2008) 105020 arXiv:0801.0578.
- [7] See H. Baer and X. Tata, *Weak Scale Supersymmetry: From Superfields to Scattering Events*, (Cambridge University Press, 2006)
- [8] J. R. Ellis, C. Kounnas and D. V. Nanopoulos, *Nucl. Phys. B* **247** (1984) 373; J. R. Ellis, A. B. Lahanas, D. V. Nanopoulos and K. Tamvakis, *Phys. Lett. B* **134** (1984) 429; G. A. Diamandis, J. R. Ellis, A. B. Lahanas and D. V. Nanopoulos, *Phys. Lett. B* **173** (1986) 303; For a review, see A. Lahanas and D. V. Nanopoulos, *Phys. Rept.* **145** (1987) 1.
- [9] D. E. Kaplan, G. D. Kribs and M. Schmaltz, *Phys. Rev. D* **62** (2000) 035010; Z. Chacko, M. A. Luty, A. E. Nelson and E. Ponton, *J. High Energy Phys.* **01** (2000) 003.
- [10] F. Gabbiani, E. Gabrielli, A. Masiero and L. Silvestrini, *Nucl. Phys. B* **477** (1996) 321.

- [11] M. Schmaltz and W. Skiba, *Phys. Rev. D* **62** (2000) 095005 and *Phys. Rev. D* **62** (2000) 095004; H. Baer, A. Belyaev, T. Krupovnickas and X. Tata, *Phys. Rev. D* **65** (2002) 075024; A. De Simone, J. J. Fan, M. Schmaltz and W. Skiba, *Phys. Rev. D* **78** (2008) 095010.
- [12] R. Dermisek and A. Mafi, *Phys. Rev. D* **65** (2002) 055002; for associated phenomenology, see H. Baer, C. Balazs, A. Belyaev, R. Dermisek, A. Mafi and A. Mustafayev, *J. High Energy Phys.* **0205** (2002) 061 and *Nucl. Instrum. Meth. A* **502** (2003) 560.
- [13] R. Dermisek, H. Verlinde and L-T. Wang, *Phys. Rev. Lett.* **100** (2008) 131804; H. Baer, R. Dermisek, S. Rajagopalan and H. Summy, *J. High Energy Phys.* **0910** (2009) 078.
- [14] J. Wess and J. Bagger, *Supersymmetry and Supergravity*, (Princeton University Press, 1992).
- [15] S. J. Gates, M. T. Grisaru, M. Rocek and W. Siegel, *Superspace, or one thousand and one lessons in supersymmetry*, *Front. Phys.* **58** (1983) 1.
- [16] S. P. de Alwis, *J. High Energy Phys.* **0903** (2009) 023 arXiv:0806.2672.
- [17] R. Blumenhagen, S. Moster and E. Plauschinn, *JHEP* **0801**, 058 (2008) [arXiv:0711.3389 [hep-th]].
- [18] R. Blumenhagen, S. Moster, and E. Plauschinn, *J. High Energy Phys.* **0801** (2008) 058.
- [19] S. P. de Alwis “Classical and Quantum SUSY Breaking Effects in IIB Local Models,” arXiv:0912.2950.
- [20] J. Bagger, T. Moroi, and E. Poppitz, *J. High Energy Phys.* **04** (2000) 009, hep-th/9911029.
- [21] V. Kaplunovsky and J. Louis, *Nucl. Phys. B* **422** (1994) 57.
- [22] N. Arkani-Hamed and H. Murayama, *J. High Energy Phys.* **0006** (2000) 030.
- [23] K. Kohri, T. Moroi and A. Yotsuyanagi, *Phys. Rev. D* **73** (2006) 123511; for an update, see M. Kawasaki, K. Kohri, T. Moroi and A. Yotsuyanagi, *Phys. Rev. D* **78** (2008) 065011; see also J. Pradler and F. D. Steffen, *Phys. Lett. B* **648** (2007) 224.
- [24] F. Paige, S. Protopopescu, H. Baer and X. Tata, hep-ph/0312045.
- [25] H. E. Haber, R. Hempfling and A. Hoang, *Z. Phys. C* **75** (1997) 539.
- [26] D. Pierce, J. Bagger, K. Matchev and R. Zhang, *Nucl. Phys. B* **491** (1997) 3.
- [27] G. Belanger, S. Kraml and A. Pukhov, *Phys. Rev. D* **72** (2005) 015003.
- [28] H.N. Brown *et al.* (Muon $g - 2$ collaboration), *Phys. Rev. Lett.* **86** (2001) 2227.
- [29] H. Baer, C. Balazs, J. Ferrandis and X. Tata, *Phys. Rev. D* **64** (2001) 035004.

- [30] T. Gherghetta, G. Giudice and J. Wells, *Nucl. Phys.* **B 559** (1999) 27; J. L. Feng, T. Moroi, L. Randall, M. Strassler and S. Su, *Phys. Rev. Lett.* **83** (1999) 1731; J. L. Feng and T. Moroi, *Phys. Rev.* **D 61** (2000) 095004; F. Paige and J. Wells, hep-ph/0001249; A. Datta and K. Huitu, *Phys. Rev.* **D 67** (2003) 115006; S. Asai, T. Moroi, K. Nishihara and T. T. Yanagida, *Phys. Lett.* **B 653** (2007) 81; S. Asai, T. Moroi and T. T. Yanagida, *Phys. Lett.* **B 664** (2008) 185; H. Baer, J. K. Mizukoshi and X. Tata, *Phys. Lett.* **B 488** (2000) 367; A. J. Barr, C. Lester, M. Parker, B. Allanach and P. Richardson, *J. High Energy Phys.* **0303** (2003) 045.
- [31] LEPSUSYWG, note LEPSUSYWG/02-04.1.
- [32] S. P. Ahlen *et al.*, *Phys. Lett.* **B 195** (1987) 603; D. Caldwell *et al.*, *Phys. Rev. Lett.* **61** (1988) 510 and *Phys. Rev. Lett.* **65** (1990) 1305; D. Reusser *et al.*, *Phys. Lett.* **B 235** (1991) 143; T. Falk, K. Olive and M. Srednicki, *Phys. Lett.* **B 339** (1994) 248.
- [33] H. Baer and M. Brhlik, *Phys. Rev.* **D 55** (1997) 3201.
- [34] M. Misiak *et al.*, *Phys. Rev. Lett.* **98** (2007) 022002.
- [35] E. Barberio *et al.* (Heavy Flavor Averaging Group), hep-ex/0603003.
- [36] H. Baer, M. Brhlik, D. Castano and X. Tata, *Phys. Rev.* **D 58** (1998) 015007.
- [37] T. Moroi and L. Randall, *Nucl. Phys.* **B 570** (2000) 455.
- [38] L. F. Abbott and P. Sikivie, *Phys. Lett.* **B 120** (1983) 133; J. Preskill, M. Wise and F. Wilczek, *Phys. Lett.* **B 120** (1983) 127; M. Dine and W. Fischler, *Phys. Lett.* **B 120** (1983) 137; M. Turner, *Phys. Rev.* **D 33** (1986) 889.
- [39] K. Rajagopal, M. Turner and F. Wilczek, *Nucl. Phys.* **B 358** (1991) 447; L. Covi, J. E. Kim and L. Roszkowski, *Phys. Rev. Lett.* **82** (1999) 4180; L. Covi, H. B. Kim, J. E. Kim and L. Roszkowski, *J. High Energy Phys.* **0105** (2001) 033; for recent reviews, see L. Covi and J. E. Kim, arXiv:0902.0769 and F. Steffen, *Eur. Phys. J.* **C 59** (2009) 557.
- [40] H. Baer, A. Box and H. Summy, *J. High Energy Phys.* **0908** (2009) 080; H. Baer and A. Box, arXiv:0910.0333 (2009).
- [41] Prospino, by W. Beenakker, R. Hopker and M. Spira, arXiv:hep-ph/9611232.
- [42] H. Baer, C. H. Chen, F. Paige and X. Tata, *Phys. Rev.* **D 49** (1994) 3283.
- [43] R. Kadala, J. K. Mizukoshi and X. Tata, *Eur. Phys. J.* **C 56** (2008) 511.
- [44] H. Baer, H. Prosper and H. Summy, *Phys. Rev.* **D 77** (2008) 055017; H. Baer, A. Lessa and H. Summy, *Phys. Lett.* **B 674** (2009) 49; H. Baer, V. Barger, A. Lessa and X. Tata, *J. High Energy Phys.* **0909** (2009) 063.
- [45] H. C. Cheng, B. Dobrescu and K. Matchev, *Nucl. Phys.* **B 543** (1999) 47.
- [46] H. Baer, C. H. Chen, F. Paige and X. Tata, *Phys. Rev.* **D 52** (1995) 2746 and *Phys. Rev.* **D 53** (1996) 6241; H. Baer, A. Belyaev, T. Krupovnickas and X. Tata, *Phys. Rev.* **D 65** (2002) 075024.